

A Novel Dual-Band Scheme for Magnetic Resonant Wireless Power Transfer

Keke Ding^{1, 2, *}, Ying Yu^{1, 2}, and Hong Lin^{1, 2}

Abstract—In this paper, a novel dual-band scheme is proposed and analyzed for dual-band magnetic resonant wireless power transfer. The scheme consists of a novel resonant coil structure for dual-band resonance and a coupling loop for dual-band impedance matching. Circuit-based analysis and experiments verify that our scheme can achieve dual-band power transfer easily and effectively, with its dual-band reflection coefficient lower than -18 dB and transmission efficiency over 37.21% at a distance of 20 cm at 6.78 MHz and 13.56 MHz.

1. INTRODUCTION

Wireless power transfer (WPT) has been a topic of interest with significant competition between technologies and standards [1–3]. The Wireless Power Consortium (WPC) organization adopts near-field inductive coupling WPT technology at 110–205 kHz and 110–300 kHz [4], while the AirFuel proposes mid-field magnetic resonant coupling (MRC) WPT with the working frequency of $6.78 \text{ MHz} \pm 15 \text{ kHz}$ [5]. Meanwhile, Industrial Scientific Medical (ISM) Band of 13.56 MHz with MRC WPT is also commonly utilized in WPT medical and wearable devices [6–8]. These different operating frequency bands would lead to incompatibility of different wireless charging products.

Dual-band or multi-band technologies might be the potential solution to this problem, and as one band can be used to transmit power as needed, the spare can be used to transmit power or data. At present, two modes have been applied to realize multi-band [9]: multi-coil mode and single-coil mode. In the multi-coil mode, the system adopts multiple resonant coils with individual frequencies to transfer concurrently [10, 11], but unwanted cross-coupling among resonant coils would cause interference among channels. [12, 13] introduce a one-coil dual-band architecture with extra series resonant circuit, but repeaters are needed to realize the dual-band impedance matching.

In this paper, we present a novel dual-band scheme with a novel coil structure and a coupling loop matching. The resonant coil is simply constructed with a lumped capacitance parallel to part of a helix coil. The coupling loop is tuned for dual-band concurrent impedance matching, with two couplings that could be tuned. Based on equivalent circuit analysis, we analyze the dual-band resonance and impedance matching principle, and develop our working WPT at 6.78 MHz and 13.56 MHz.

2. THE DUAL-BAND SCHEME

2.1. Dual-Band Resonant Coil Structure

The basic structure of our dual-band resonant coil and its equivalent circuit is illustrated in Figure 1. The resonant coil consists of a helix coil and an external lumped capacitance (C_1). The lumped capacitance

Received 22 August 2018, Accepted 12 November 2018, Scheduled 23 November 2018

* Corresponding author: Keke Ding (dingkekedkk@163.com).

¹ College of Electronic Science and Engineering, Nanjing University of Posts and Telecommunications, Nanjing, Jiangsu 210023, China. ² National and Local Joint Engineering Laboratory of RF Integration and Micro-assembly Technology, Nanjing, Jiangsu 210023, China.

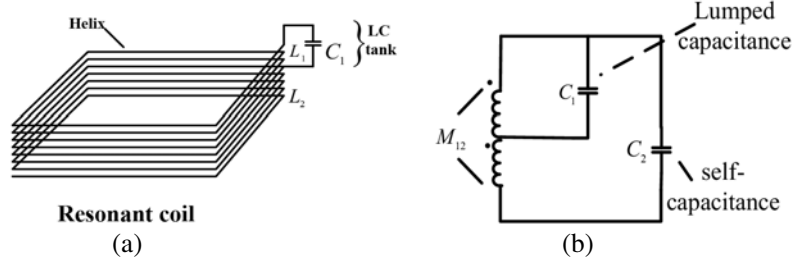


Figure 1. The dual-band resonant coil. (a) Coil structure. (b) Equivalent circuit.

(C_1) and part of the helix coil inductance make up the LC tank (parallel resonant). The rest inductance series with LC tank are connected in parallel with the helix coil self-capacitance (C_2). Mutual inductance M_{12} between two parts of the helix coil is also included in the equivalent circuit for more accuracy.

The structure is chosen for the two main reasons. Firstly, it is simple to implement. We can achieve the desired resonant frequencies by adding an appropriate capacitance C_1 to a helix coil. Secondly, the self-inductance of the helix coil participates in both coupling band, but the couplings of a loop to two parts of the helix coil are not the same, so a coupling loop could be set inside the resonant coil to adjust the port impedance for dual-band concurrent impedance matching, as depicted in Figure 3(b).

2.2. Resonant Frequency Analysis and Coil Design Guideline

According to the decoupling equivalent method, the equivalent circuit in Figure 1(b) can be decoupled to Figure 2(a). Both L_1 and L_2 contain the self-inductance and mutual-inductance in between, so $L_1 > M_{12}$, $L_2 > M_{12}$.

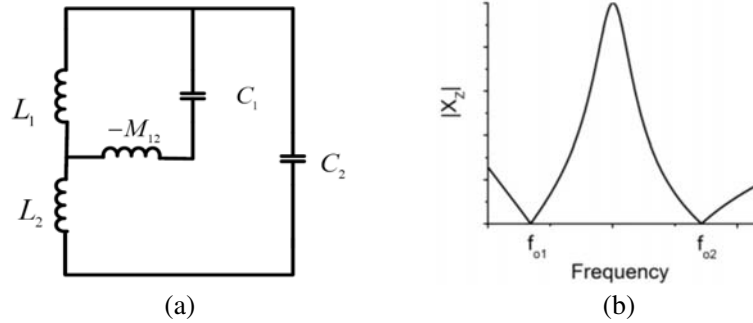


Figure 2. The dual-band resonant coil frequency analysis. (a) Decoupled equivalent circuit. (b) Frequency response of the coil impedance reactance.

The frequency response of the coil impedance reactance is depicted in Figure 2(b). There are two zeros in the impedance reactance.

$$X_Z = j\omega L_1 // \left(\frac{1}{j\omega C_1} - j\omega M_{12} \right) + j\omega L_2 + \frac{1}{j\omega C_2} \quad (1)$$

Solving $X_Z = 0$, the resonant frequencies can be obtained by Eqs. (2)–(4) with corresponding coil parameters.

$$f_{o1} = \frac{1}{2\pi} \left(\frac{B - \sqrt{B^2 - 4A}}{2A} \right)^{\frac{1}{2}} \quad (2)$$

$$f_{o2} = \frac{1}{2\pi} \left(\frac{B + \sqrt{B^2 - 4A}}{2A} \right)^{\frac{1}{2}} \quad (3)$$

where

$$\begin{cases} A = L_1 L_2 C_1 C_2 - M_{12} L_2 C_1 C_2 - L_1 M_{12} C_1 C_2 \\ B = L_1 C_1 - M_{12} C_1 + L_2 C_2 + L_1 C_2 \end{cases} \quad (4)$$

And our resonant coil at the required resonant frequencies f_{o1} f_{o2} can be designed with the following steps.

Step 1: construct an original helix coil with self-resonant frequencies within the range $[f_{o1}, f_{o2}]$, and measure the self-inductance L ($L = L_1 + L_2$) and self-capacitance C_2 .

Step 2: select the turn number n_{L_1} of L_1 , and measure L_1 , L_2 , M_{12} . Integer n_{L_1} is preferred to facilitate the welding of C_1 .

Step 3: using the numerical searching method with MATLAB and formulas (2) (3), find the suitable C_1 and L_2 to make calculated resonant frequencies in the required bands. Noted that L_2 should be searched in small range, so that L_1 and M_{12} could be approximately assumed to be unchanged. If no suitable value is found, repeat step 2 and step 3 with another n_{L_1} .

Step 4: construct the resonant coil with the calculated C_1 and n_{L_1} . Considering the approximation of the equivalent circuit, fine-tune C_1 , L_1/L_2 (the pin position of C_1) to finally meet the required resonance.

2.3. Dual-Band Impedance Matching

In wireless power transfer systems, the optimum power transfer efficiency (PTE) can be achieved when the impedance matching is achieved [13]. However, the dual-frequency impedance matching is difficult in dual-band systems. Multi-coils [10] or repeaters [12] have been used to implement the dual-band impedance matching, which increases the complexity of the system. Here we utilize the couplings between our resonant coils and coupling loops, similar to the coils in four-coil WPT systems [14]. The coupling loop in the transmitter (TX) is connected to the power source, and it acts as a load loop in the receiver (RX), as depicted in Figure 3(a). Since TX and RX are identical, only the input impedance matching in TX is discussed here. Load matching in RX is similar.

When the TX and RX are apart far enough, the coupling coefficient of TX and RX has little influence on the input impedance. So the input impedance could be estimated by the equivalent circuit of TX in Figure 3(b). M_{01} is the mutual inductance between the coupling loop and L_1 . M_{02} is the mutual inductance between the loop and L_2 . According to the circuit theory, the TX equivalent equation can be written as

$$\begin{cases} U_{in} = (X_{L_0} + R_0) i_0 + j\omega M_{01} i_1 + j\omega M_{02} i_2 \\ (Z_1 - j\omega M_{12}) i_1 - i_2 (X_{C_1} - j\omega M_{12}) = j\omega M_{01} i_0 \\ Z_2 i_2 + (X_{C_1} - j\omega M_{12}) (i_2 - i_1) = j\omega M_{02} i_0 \end{cases} \quad (5)$$

where $X_{L_m} = j\omega L_m$, $X_{C_m} = \frac{1}{j\omega C_m}$, $Z_m = X_{L_m} + X_{C_m} + R_m$, R_m are the parasitic resistance ($m = 0, 1, 2$). So the input impedance can be expressed as

$$Z_{in} = \frac{U_{in}}{i_0} = (X_{L_0} + R_0) + \frac{M_{01}^2 (Z_2 + X_{C_1} - j\omega M_{12}) + M_{02}^2 (Z_1 - j\omega M_{12}) + 2M_{01} M_{02} (X_{C_1} - j\omega M_{12})}{(Z_1 - j\omega M_{12}) (Z_2 + X_{C_1} - j\omega M_{12}) - (X_{C_1} - j\omega M_{12})^2} \omega^2 \quad (6)$$

From Equation (12), we can see that when the resonant coil has been determined, the input impedance Z_{in} is a function of M_{01} and M_{02} . Choosing the appropriate M_{02}/M_{01} , Z_{in} can be tuned to be identical at the two resonant frequencies, as shown in the example in Figure 3(c).

According to Neumann's formula, M_{01} and M_{02} can be controlled by the size of the coupling loop and the distance between the loop and L_1 and L_2 [8]. Therefore, by carefully adjusting the size and position of the coupling loop, we can adjust the ratio of M_{02}/M_{01} and tune the port impedances to achieve concurrent dual-band impedance matching.

It needs to be noted that the analysis above is under the condition that the coupling between TX and RX is small enough to be omitted. When the coupling is large, frequency splitting phenomenon would take place [15], which is not discussed here.

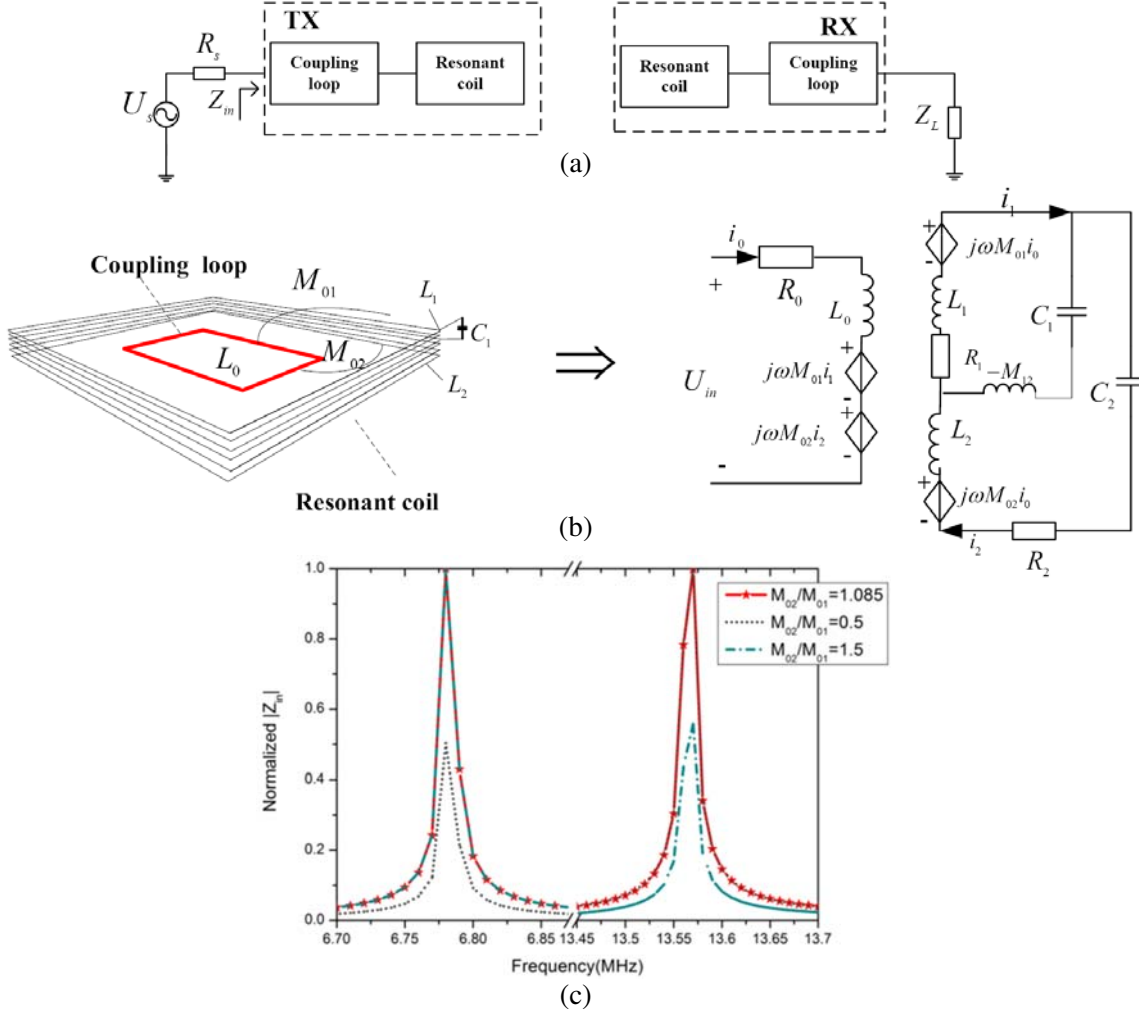


Figure 3. Dual-band impedance matching scheme. (a) Block diagram of our proposed scheme. (b) The structure and equivalent circuit of the TX. (c) Normalized input impedance with the varied M_{02}/M_{01} . ($C_1 = 106$ pF, $L_1 = 8.66$ μ H, $C_2 = 5.3$ pF, $L_2 = 52.6$ μ H, $M_{12} = 5.24$ μ H, $R_1 = 0.11$ Ω , $R_2 = 0.54$ Ω . These are coil parameters in the simulation model. It is found that when M_{02}/M_{01} is close to 1.085, two $|Z_{in}|$ are close to each other at two resonant frequencies.)

3. EXPERIMENT AND VERIFICATION

The experimental setup is depicted in Figure 4. Rectangular helix coil is chosen for easy implementation. The resonant coils are initially fabricated according to the simulation, then tuned to resonate at the desired 6.78 MHz and 13.56 MHz, following the steps mentioned in Subsection 2.2. The measured values of L_1 , L_2 , M_{12} and C_2 are 8.29 μ H, 53.24 μ H, 5.04 μ H and 6.4 pF. The parasitic resistors of L_1 , L_2 are 0.56 Ω and 2.61 Ω . The coupling loop is wrapped on a movable holder, inserted inside the helix coil, and tuned to be port matched. The wire is made of copper, with a diameter of 1 mm. The structure parameters in the experiment and simulation are listed in Table 1. Because of the inconsistency in manual production, TX and RX are slightly different. TX and RX are aligned coaxially and separated by a distance of d .

System performance is evaluated in the S -parameters with a vector network analyzer (VNA, TD3618C) measurement and simulation, where S_{11} and S_{21} represent the wave reflection and transmission ratios. System power transfer efficiency can be evaluated as $\text{PTE} = |S_{21}|^2 / (1 - |S_{11}|^2) \approx |S_{21}|^2$ [12].

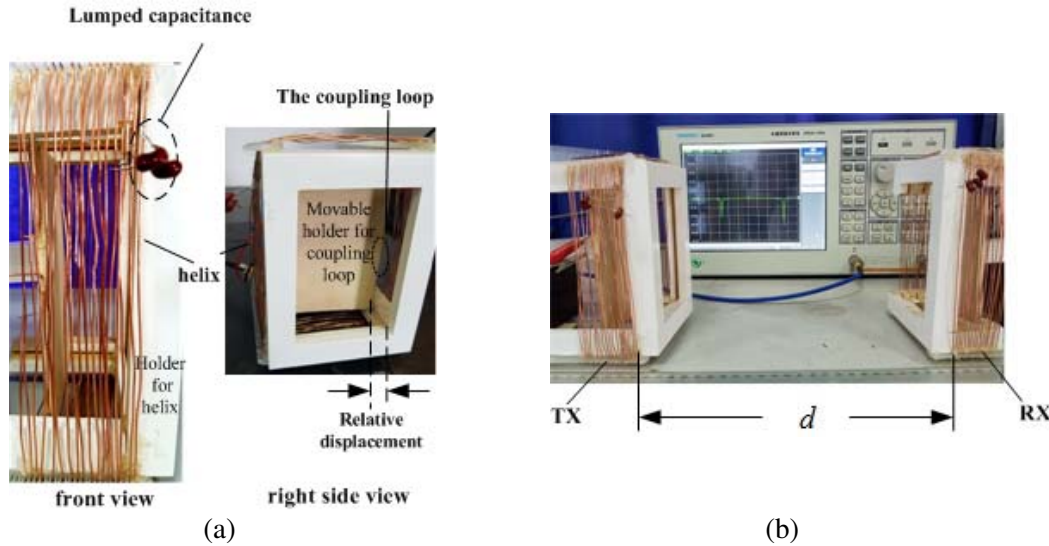


Figure 4. The experimental setup. (a) Fabricated resonant coil and coupling loop. (b) Measurement setup.

Table 1. Structure parameters in the experiment and simulation.

	Resonant coil				Coupling Loop	Relative displacement (cm)	C_1 (pF)
	Length /width (cm)	Height (cm)	Turns	n_{L_1}/n_{L_2} (turns)	Length/width (cm)		
Experiment (TX)	16/12	5	17.5	3/14.5	12.5/8	4.2	80
Experiment (RX)	16/12	4.8	17	3/14	12.5/8	4.0	84
Simulation	16/12	5.1	17.2	3/14.2	12.5/8	2.1	106

The length and height of the resonant coil are the sides of the rectangular helix coil. n_{L_1}/n_{L_2} is the turns of the coil. Relative displacement is the distance between the coupling loop and the resonant coil (L_1 side) as depicted in Figure 3(a).

Figure 5 shows the graph of measured and simulated S-parameters when $d = 20$ cm. The measured S_{11} results show that $|S_{11}|$ is less than -18 dB at 6.78 MHz and less than -25 dB at 13.56 MHz, meaning that the reflected power is less than 1% at dual bands. This means that the impedance are successfully matched. $|S_{21}|$ in the lower band is greater than in the higher band. It might be because the current directions in L_1 and L_1 are the same in lower band, while they are reversal in higher band [16], which cause the field to increase in lower band and decrease in higher band. Though the measured $|S_{21}|$ is not good enough, 49.14% PTE at 6.78 MHz and 37.21% PTE at 13.56 MHz are obtained. Frequency splitting [17] takes place in simulated S-parameters, due to its much higher quality (Q) than that in the experiment.

Figure 6 shows how $|S_{21}|$ and PTE vary with the distance d between TX and RX. When distance d is small, the frequency splitting takes place, which reduces the PTE at the desired frequencies. As d increases, the splitting frequencies merge into one, achieving the maximum efficiency. Then, if d gets even larger, the transfer efficiency drops. Maximum efficiency measured at 6.78 MHz is 51.4% at $d = 17.5$ cm, and the maximum at 13.56 MHz is 46.92% at $d = 15$ cm.

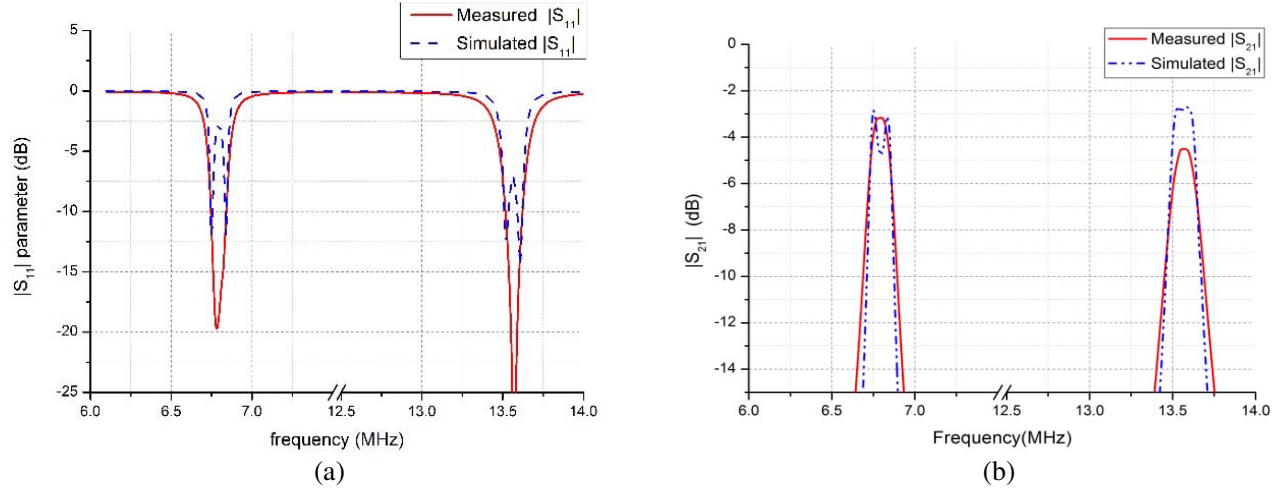


Figure 5. Measured and simulated S -parameters when $d = 20$ cm. (a) S_{11} result. (b) S_{21} result.

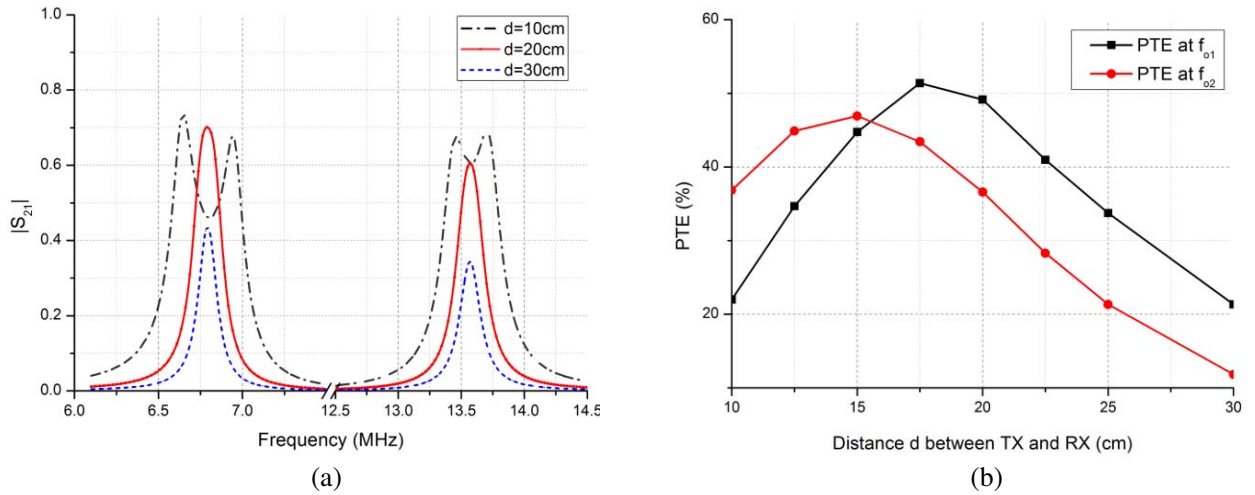


Figure 6. Dual-band WPT results from 10 cm to 30 cm. (a) S_{21} result. (b) PTE result.

4. CONCLUSION

We propose a novel dual-band WPT scheme in this paper. Compared with previous researches, our single resonant coil structure can reduce the cross-coupling effect in multi-coil systems, and coupling loop can provide ways to concurrent dual-band impedance matching. Simulation and experiments show that it can transfer power efficiently in each band channel with matched impedance. It provides a feasible and effective scheme to realize dual-band WPT.

Future research efforts will focus on the optimization of the structure to further increase PTE and reduce the coil size.

ACKNOWLEDGMENT

This work was supported by the Research Innovation Program for College Graduates of Jiangsu Province (CXZZ12_0460), the Open Research Fund of State Key Lab. of Millimeter Wave (K201412) and the National Natural Science Foundation of China (61302155).

REFERENCES

1. Covic, G. A. and J. T. Boys, "Inductive power transfer," *Proceedings of the IEEE*, Vol. 101, No. 6, 1276–1289, Jun. 2013.
2. Badawe, M. El. and O. M. Ramahi, "Efficient meta surface rectenna for electromagnetic wireless power transfer and energy harvesting," *Progress In Electromagnetics Research*, Vol. 161, 35–40, 2018.
3. Jang, B. J., S. Lee, and H. Yoon, "HF-band wireless power transfer system: concept, issues, and design," *Progress In Electromagnetics Research*, Vol. 124, 211–231, 2012.
4. Johns, B. B., "An introduction to the wireless power consortium standard and TI's compliant solutions," *Analog Applications Journal*, 10–12, 1Q. 2011
5. Alliance, A., "A4WP wireless power transfer system baseline system specification (BSS) v 1.2.1," 2014.
6. Chen, J.-F., Z. Ding, Z. Hu, S. Wang, Y. Cheng, M. Liu, B. Wei, and S. Wang, "Metamaterial-based high-efficiency wireless power transfer system at 13.56 MHz for low power applications," *Progress In Electromagnetics Research B*, Vol. 72, 17–30, 2017.
7. Li, X., C. Y. Tsui, and W. H. Ki, "A 13.56 MHz wireless power transfer system with reconfigurable resonant regulating rectifier and wireless power control for implantable medical devices," *2014 Symposium on VLSI Circuits Digest of Technical Papers*, 1–2, 2014.
8. Kim, J., W. S. Choi, and J. Jeong, "Loop switching technique for wireless power transfer using magnetic resonance coupling," *Progress In Electromagnetics Research*, Vol.138, 197–209, 2013.
9. Kung, M. L. and K. H. Lin, "Investigation of dual-band coil module for near-field wireless power transfer systems," *Wireless Power Transfer Conference*, 265–268, 2014.
10. Ahn, D. and P. P. Mercier, "Wireless power transfer with concurrent 200-kHz and 6.78-MHz operation in a single-transmitter device," *IEEE Transactions on Power Electronics*, Vol. 31, No. 7, 5018–5029, 2016.
11. Jiang, C., K. T. Chau, W. Han, and W. Liu, "Development of multilayer rectangular coils for multiple-receiver multiple-frequency wireless power transfer," *Progress In Electromagnetics Research*, Vol. 163, 15–24, 2018.
12. Kung, M. L. and K. H. Lin, "Dual-band coil module with repeaters for diverse wireless power transfer applications," *IEEE Transactions on Microwave Theory & Techniques*, Vol. 66, No. 1, 332–345, 2018.
13. Kung, M. L. and K. H. Lin, "Enhanced analysis and design method of dual-band coil module for near-field wireless power transfer systems," *IEEE Transactions on Microwave Theory and Techniques*, Vol. 63, No. 3, 821–832, 2015.
14. Kurs, A., A. Karalis, R. Moffatt, J. D. Joannopoulos, P. Fisher, and M. Soljacic, "Wireless power transfer via strongly coupled magnetic resonances," *Sci. Exp.*, Vol. 317, No. 5834, 83–86, Jun. 2007.
15. Peng, L., O. Breinbjerg, and N. A. Mortensen, "Wireless energy transfer through non-resonant magnetic coupling," *Journal of Electromagnetic Waves and Applications*, Vol. 24, 1587–1598, 2010.
16. Kim, J. G., G. Wei, C. Zhu, and C. H. Rim, "Quality factor and topology analysis of the series-parallel combined resonant circuit-based wireless power transfer system," *IEEE Transportation Electrification Conference and Expo.*, 2017.
17. Peng, L., J. Y. Wang, L. X. Ran, O. Breinbjerg, and N. A. Mortensen, "Performance analysis and experimental verification of mid-range wireless energy transfer through non-resonant magnetic coupling," *Journal of Electromagnetic Waves and Applications*, Vol. 25, 845–855, 2011.